Title

High-brightness X-ray free-electron laser with an optical undulator by pulse shaping.

Permalink

https://escholarship.org/uc/item/5f41k1wj

Authors

Chang, Chao
Liang, Jinyang
Hei, Dongwei
et al.

High-brightness X-ray free-electron laser with an optical undulator by pulse shaping

Chao Chang,[1,2,7] **Jinyang Liang,**[3,4,7] **Dongwei Hei,**[2] **Michael F. Becker,**[4] **Kelei Tang,**[5] **Yiping Feng,**[1] **Vitaly Yakimenko,**[1] **Claudio Pellegrini,**[1,6] **and Juhao Wu**[1,*]

[1]*SLAC National Accelerator Laboratory, Stanford University, Stanford, CA 94309, USA,*
[2]*Institute of Energy, Tsinghua University, Beijing 100084, China,* [3]*Department of Biomedical Engineering, Washington University in St. Louis, St. Louis, MO 63130, USA,* [4]*Department of Electrical and Computer Engineering, The University of Texas at Austin, Austin, TX 78712, USA,* [5]*Monta Vista High School, Cupertino, CA 95014, USA,* [6]*Department of Physics and Astronomy, University of California Los Angeles, Los Angeles, CA 90095, USA,*
[7]*These authors contribute equally to this work*
[*]*Corresponding author: jhwu@slac.stanford.edu*

Abstract: A normal-incident flattop laser with a tapered end is proposed as an optical undulator to achieve a high-gain and high-brightness X-ray free electron laser (FEL). The synchronic interaction of an electron bunch with the normal incident laser is realized by tilting the laser pulse front. The intensity of the flattop laser is kept constant during the interaction time of the electron bunch and the laser along the focal plane of a cylindrical lens. Optical shaping to generate the desired flattop pulse with a tapered end from an original Gaussian pulse distribution is designed and simulated. The flattop laser with a tapered end can enhance the X-ray FEL beyond the exponential growth saturation power by one order to reach 1 Gigawatt as compared to that without a tapered end. The peak brightness can reach 10^{30} photons/mm^2/mrad^2/s/0.1% bandwidth, more than 10 orders brighter than the conventional incoherent Thompson Scattering X-ray source.

© 2013 Optical Society of America

OCIS codes: (140.2600) Free-electron lasers (FELs); (140.3300) Laser beam shaping; (050.2770) Gratings; (290.0290) Scattering.

References and links

1. P. Emma, R. Akre, J. Arthur, R. Bionta, C. Bostedt, J. Bozek, A. Brachmann, P. Bucksbaum, R. Coffee, F.-J. Decker, Y. Ding, D. Dowell, S. Edstrom, A. Fisher, J. Frisch, S. Gilevich, J. Hastings, G. Hays, Ph. Hering, Z. Huang, R. Iverson, H. Loos, M. Messerschmidt, A. Miahnahri, S. Moeller, H.-D. Nuhn, G. Pile, D. Ratner, J. Rzepiela, D. Schultz, T. Smith, P. Stefan, H. Tompkins, J. Turner, J.Welch, W. White, J. Wu, G. Yocky, and J. Galayda, "First lasing and operation of an Ångström-wavelength free electron laser," Nature Photonics **4**, 641-647 (2010) and references therein.
2. J. Bahrdt and Y. Ivanyushenkov, "Short Period Undulators for Storage Rings and Free Electron Lasers," Journal of Physics: Conference Series **425**, 032001 (2013).
3. M. Shumail, G. Bowden, C. Chang, J. Neilson, and S. Tantawi, "Beam dynamics studies of a helical X-band RF undulator," AIP Conf. Proc. **1507**, 752-756 (2012).
4. V. Petrillo, L. Serafini, and P. Tomassini, "Ultrahigh brightness electron beams by plasma-based injectors for driving all-optical free-electron lasers," Phys. Rev. Spec. Top. Accel. Beams **11**, 070703 (2008).
5. P. Sprangle, B. Hafizi, and J.R. Peñano, "Laser-pumped coherent x-ray free-electron laser," Phys. Rev. Spec. Top. Accel. Beams **12**, 050702 (2009).

6. P.R. Ribic and G. Margaritondo, "The physics behind free electron lasers (FELs) based on magnetostatic and optical undulators," Phys. Status Solidi B **249**, 1210 (2012).
7. J. Hecht, "Fiber lasers: The State of the art," Laser Focus World **48**, 57-60 (2012).
8. C. Chang, C. Tang, and J. Wu, "High-Gain Thompson-Scattering X-Ray Free-Electron Laser by Time-Synchronic Laterally Tilted OpticalWave," Phys. Rev. Lett. **110**, 064802 (2013).
9. A.D. Debus, S. Bock, M. Bussmann, T.E. Cowan, A. Jochmann, T. Kluge, S.D. Kraft, R. Sauerbrey, K. Zeil, and U. Schramm, "Linear and Non-Linear Thomson-Scattering X-Ray Sources Driven by Conventionally and Laser Plasma Accelerated Electrons," Proc. SPIE Int. Soc. Opt. Eng. **7359**, 735908 (2009).
10. J.E. Lawler, J. Bisognano, R.A. Bosch, T.C. Chiang, M.A. Green, K. Jacobs, T. Miller, R. Wehlitz, D. Yavuz, and R.C. York, "Nearly copropagating sheared laser pulse FEL undulator for soft x-rays," J. Phys. D: Appl. Phys. **46**, 325501 (2013).
11. J. Liang, R.N. Kohn, Jr., M.F. Becker, and D.J. Heinzen, "High-precision laser beam shaping using a binary-amplitude spatial light modulator," Applied Optics **49**, 1323-1330 (2010).
12. L.H. Yu, S. Krinsky, R.L. Gluckstern, and J.B.J. van Zeijts, "EfFect of wiggler errors on free-electron-laser gain," Phys. Rev. A **45**, 1163-1174 (1992).
13. S.-W. Bahk, E. Fess, B.F. Kruschwitz, and J.D. Zuegel, "A high-resolution, adaptive beam-shaping system for high-power lasers," Opt. Express **18**, 9151-9162 (2010).
14. C. Pellegrini and S. Reiche, "The Development of X-Ray Free-Electron Lasers," IEEE J. Sel. Top. Quantum Electron. **10**, 1393-1404 (2004).
15. N.M. Kroll, P.L. Morton, and M.N. Rosenbluth, "Free-Electron Lasers with Variable Parameter Wigglers," IEEE J. Quantum Electronics, **QE-17**, 1436-1468 (1981).
16. Y. Jiao, J. Wu, Y. Cai, A.W. Chao, W.M. Fawley, J. Frisch, Z. Huang, H.-D. Nuhn, C. Pellegrini, and S. Reiche, "Modeling and multidimensional optimization of a tapered free electron laser," Phys. Rev. Spec. Top. Accel. Beams **15**, 050704 (2012)
17. K.T. Knox, "Error image in error diffusion," Proc. SPIE, vol. 1657, pp.268-279 (1992)
18. S. Reiche, "GENESIS 1.3: a fully 3D time-dependent FEL simulation code," Nucl. Instr. Meth. A **429**, 243-248 (1999).
19. F. Li, J.F. Hua, X.L. Xu, C.J. Zhang, L.X. Yan, Y.C. Du, W.H. Huang, H.B. Chen, C.X. Tang, W. Lu, C. Joshi, W.B. Mori, and Y.Q. Gu, "Generating High-Brightness Electron Beams via Ionization Injection by Transverse Colliding Lasers in a Plasma-Wakefield Accelerator," Phys. Rev. Lett. **111**, 015003 (2013).
20. Z. Huang, Y. Ding, and C. Schroeder, "Compact X-ray Free-Electron Laser from a Laser-Plasma Accelerator Using a Transverse-Gradient Undulator," Phys. Rev. Lett. **109**, 204801 (2012)
21. S.G. Anderson, C.P.J. Barty, S.M. Betts, W.J. Brown, J.K. Crane, R.R. Cross, D.N. Fittinghoff, D.J. Gibson, F.V. Hartemann, J. Kuba, G.P. Lesage, J.B. Rosenzweig, D.R. Slaughter, P.T. Springer, and A.M. Tremaine, "Short-pulse, high-brightness X-ray production with the PLEIADES Thomson-scattering source," Appl. Phys. B **78**, 891-894 (2004).

Free-electron lasers (FEL) are the most powerful X-ray radiation sources to support many frontier researches [1]. For the existing X-ray FEL facilities, electron bunches with multi-GeV energy and magnetostatic undulator sections with tens of meters long are required [1]. Shortening the undulator period can shorten the undulator length, and also make it possible to use electron bunches with much lower energy than multi-GeV level. Along this line of research, superconductiong undulator can shorten the period by a few times as compared to the period of a magnetostitic undulator [2]. Microwave undulator is also making great progress to have undulator period comparable to that of superconducting undulator [3]. However, to have an undulator period which is several order-of-magnitude shorter than that of the above mentioned devices, an optical undulator [4–6] is promising and can realize the X-ray FEL with a multi-MeV electron bunch within a centimeter long interaction length. With rapid progress in generating a table-top terawatt laser pulse and fiber optics, the optical undulator can provide effective magnetic field B_u on the order of kilo-Tesla, which can provide strong enough effective undulator strength K for lasing [7]. The effective undulator strength is defined as $K = eB_u\lambda_u/(2\pi m_e c) = eE_u\lambda_u/(2\pi m_e c^2)$ with e, m_e being the electron charge and mass, c the speed of light in vacuum, B_u the magnetic field, E_u the electrical field, and λ_u the undulator period. For head-on collision of an electron bunch and a laser, the interaction time between a close-to-speed-of-light electron bunch and a counter-propagating laser depends mainly on the laser pulse duration. To realize an optical undulator with a 10-20 FEL gain length, *i.e.*, typically

3 cm long, a 6 cm (or 200 ps) long counter-propagating laser pulse is required. To increase the laser intensity or the effective undulator strength K value, the incident laser is strongly focused transversely. This can be seen clearly from the definition of a Gaussian laser beam power, *i.e.*, $P_0 = \pi w_0^2 E_u^2 / (4Z_0)$ with w_0 the transverse waist size, and Z_0 the vacuum impedance. For a given laser power P_0, if we want to increase the effective undulator strength $K \propto E_u$, we will have to decrease w_0, *i.e.*, through strong focusing. However, the tighter the focus, the larger the divergence, and the shorter the Rayleigh range, $Z_R = \pi w_0^2 / \lambda_u$. Therefore, the laser beam size $w(z)$ changes quickly with travel distance z, *i.e.*, $w(z) = w_0 \sqrt{1 + (z/Z_R)^2}$. So, at any interaction instant, the local electric field changes quickly, *i.e.*, $E_u(z) \propto 1/w(z)$. Therefore, the local undulator strength, $K(z) \propto E_u(z)$, varies significantly during the head-on interaction of an electron bunch and a laser. This rapid variation is fatal for a high-gain FEL, which needs to maintain the required resonance condition $\lambda_r = \lambda_u (1 + K^2/2)/(2\gamma^2)$, *i.e.*, to keep lasing at the same wavelength λ_r, the undulator strength K should be kept constant for a given γ, the electron's Lorentz relativistic factor. To resolve such a quandary, we have to decouple the focusing of the laser beam from enlengthening the interaction time. One solution is to configure a normal incident laser with a tilted pulse front as shown in Fig. 1, where the laser is focused in the y-direction; while the electron-laser synchronic interaction is in the x-z plane with $y = 0$. The laser is shown as the parallelogram $\overline{ABCD}$ with a duration of a few cycles only in the propagation z-direction, *e.g.*, $\overline{CD} = 5\lambda_u$, but the interaction length can be extended to a few hundreds cycles, *e.g.*, $\overline{AB} = 500\lambda_u$, so that the electron-laser synchronic interaction time can be extended by several orders [8, 9]. The cylindrical focusing lens focuses the laser in the y-direction with $\overline{PQ}$ indicating the focal point, then during the interaction time the electron bunch shown as the green ellipse will experience a strong focused effective undulator strength. This concept is further generalized for soft X-ray generation with a nearly copropagating sheared laser pulse [10]. In this paper, we give a novel design of the tilted pulse front approach for realizing such a compact high-gain FEL with optical undulator. We also theoretically demonstrate that the energy efficiency and FEL power could be further improved beyond the saturation of the exponential growth by adopting a tapered optical field with a tilted pulse front. Thus, the brightness of the FEL can be further enhanced. For relativistic electrons with a velocity close
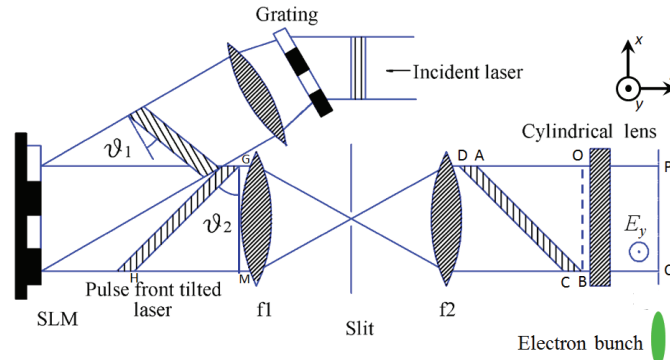

Fig. 1. Schematic of a X-ray FEL. SLM, spatial light modulator; f1-f2, lenses.

to the speed of light, to maintain synchronous interaction means that $\overline{OA}/c = \overline{OB}/(\beta c)$ as in Fig. 1, where the electron is traveling along $\overline{QP}$ with a speed of βc. Since $\overline{QP} = \overline{OB}$, for $\beta \to 1$, the triangle ΔOAB is almost an isosceles triangle, with $\overline{OA} \approx \overline{OB}$. The tilted angle $\vartheta_2 = \angle MGH$ is defined as the angle between the pulse front $\overline{GH}$, and the phase front $\overline{GM}$. As long as the synchronous interaction is satisfied, the titled angle ϑ_2 can be arbitrary [10]. In this paper, the titled angle ϑ_2 is chosen to be close to 45 degree [8]. In our design, ϑ_2 is created by using optical diffractive elements with angular dispersion as in Fig. 1. The incident laser first passes

the grating and acquires a pulse front tilt of ϑ_1 with respect to the phase front. The laser then passes a spatial light modulator (SLM) [11]. By the high-precision optical pulse shaping based on SLM, the transverse intensity profile of the laser is transformed from an incident Gaussian to a flattop profile with a tapered end. The design details will be elaborated below. Because FELs require a high-precision beam pattern with uniform effective undulator strength [12], here we use SLM-based pulse shaping to achieve high-precision. The SLM device consists of an array of aluminum-coated micromirrors. The damage threshold of the SLM for the high power laser could reach 1 J/cm^2 [13]. The power capacity can be higher if the aluminum film is replaced by a gold film. Each micromirror can be latched in two positions, at $\pm$12-degree from the SLM surface normal. When operating with a coherent source, the SLM functions as a programmable blazed gratings whose diffraction characteristics can be analyzed based on the wavelength, the blazed angle, and the pixel size [11]. Therefore, the laser pulse front tilt can be further increased as in Fig. 1, and the effective interaction length $\overline{BA}$ is extended to the entire transverse width of the laser pulse. The electric field, shown as E_y in Fig. 1, has polarization along the y-axis. Moreover, the electron bunch moves along $\overline{QP}$, $i.e.$, the focal plane of a cylindrical lens in the y-direction as in Fig. 1. The intensity of the flattop laser along the electron's path has a constant section with a length of centimeters. Compared to laser period on micron level, this interaction length is long enough to realize the FEL exponential growth, leading to a significantly enhanced coherent radiation based on the simulation below. In the optical layout of a SLM-based pulse shaper as in Fig. 1, the input pulse with a ϑ_1-degree pulse front tilt is formed by one angular gratings and is collimated by a convex lens. In our design $\vartheta_1 = 21$ degree. The input laser pulse is then incident on the SLM. Because the transverse profile of the pulse-front-tilted laser arrives at different time, each section of the transverse profile is modulated consecutively by individual row (or column) of the binary SLM pattern. A slit placed at the back focal plane of the first lens (f1) performs one-dimensional spatial filtering that cleans out most of the spatial noise introduced by the binary amplitude modulation in pulse shaping. As a result, the modulated beam is converted to the desired profile in the filtering direction while maintaining spatial sharpness (as a row or column) in the non-filtering direction. Besides, as a blazed gratings with the tilt angle of 12-degree, SLM leads to an additional pulse front tilt of 24 degree after its reflection. Thus, the final tilted pulse front angle reaches $\vartheta_2 \sim 45$ degree as required in Fig. 1.

Once we have an optical laser with uniform field distribution as described above, we can design a FEL whose exponential growth saturation power depends on the undulator field strength, the electron bunch current, energy, and qualities such as energy spread and emittance [14]. During the FEL exponential growth process, due to energy conservation, the energy of the electrons ($\gamma m_e c^2$) decreases when electrons continuously radiate X-ray photons. According to the resonant condition $\lambda = \lambda_u(1 + K^2/2)/(2\gamma^2)$, to further extract energy from the electron bunch at λ, one has to decrease the undulator strength K synchronously for a decreasing γ [15]. In the following, for SLM-based pulse shaping, we use the taper profile [16]: $K(z) = K(z_0)\left[1 - a(z - z_0)^2/(L - z_0)^2\right]$ for $z > z_0$, where z_0 indicates the taper starting point, L is the tapered optical undulator length, a is the taper amplitude, and K as mentioned above is the effective undulator strength from the laser field. For $z < z_0$, K is constant. In simulation, the field size is 52.6×52.6 mm^2 for a laser with wavelength of $\lambda_u = 10$ μm. The incident laser pulse transverse profile follows a Gaussian distribution [$G(y,z)$] with the $1/e^2$ beam width of $R_G = 5.25$ mm. The target profile $T(y,z)$ is generated by multiplying the tapered field $K(z)$ (with $z_0 = 26.28$ mm and $L = 13.68$ mm) with an 8th-order Super Lorentzian flattop function. The input Gaussian profile $G(y,z)$ and the target distribution $T(y,z)$ are:

$$G(y,z) = G_0 \exp\left(-2[y^2 + z^2]/R_G^2\right), \text{ and } T(y,z) = K(z)SL_0\left[1 + \left(\sqrt{y^2 + z^2}/R_{SL}\right)^8\right]^{-1} \text{ where}$$

G_0 is the normalized intensity at the Gaussian profile center ($G_0 = 1$), $SL_0 = 0.34K(z_0)$, and

$R_{SL} = 18.60$ mm. This target profile has the required uniform intensity distribution at the center to ensure FEL exponential growth. In addition, it has smooth transition areas to zero intensity to serve as a tapered undulator. This confines the bandwidth of the target function at low spatial frequency range for high-precision pulse shaping. The view against the laser propagation direction for the ideal goal profile is shown in Fig. 2(a). These parameters give the pulse shaping principle and a target image that does not exceed the input Gaussian in intensity [Fig. 2(b)]. The target profile in Fig. 2(a) is used to generate the SLM pattern in the optical system
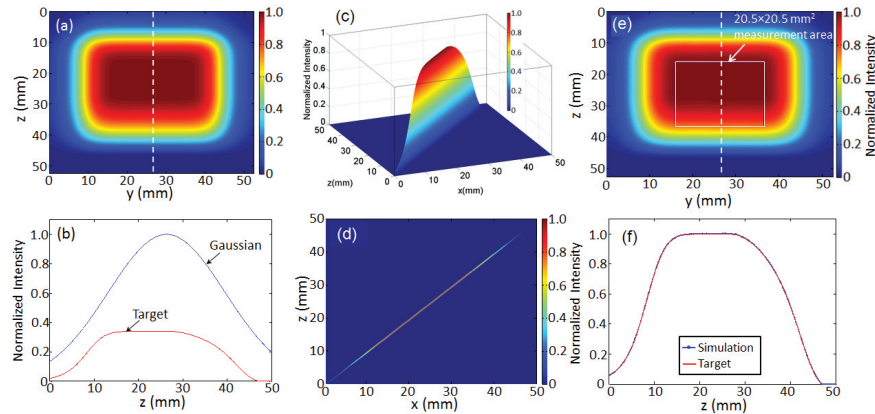

Fig. 2. (a) Front view and (b) cross sections of the target image (dash line in (a)) and the incident Gaussian profile; (c) 3D and (d) 2D plot of the maximal intensity projection of the simulated shaped tilt pulse in the x-z plane; (e) Front view and (f) cross sections (along the dash line in (e)) of the simulated shaped tilt pulse (blue dot-dashed curve) with the target image (red solid curve). Shown here, the beam profile is before the cylindrical lens.

illustrated in Fig. 1. The binary SLM pattern is initially designed using the one-dimensional error diffusion algorithm [17] and can be improved by the iterative pattern refinement [11]. As a digital halftoning technique, the error diffusion algorithm converts the continuous reflectance profile to the binary SLM pattern. The generated binary pattern has blue-noise characteristics, meaning the majority of noise locates at high spatial frequency range, while the image content at middle and low spatial frequency ranges is well preserved. The optimized slit width corresponds to the normalized system bandwidth $f_n = 0.012$. The slit filters out most high spatial frequency noise and keeps the major image content. As a result, a grayscale output image is produced with high precision. The transverse profile quality of the shaped pulse is quantified by the root-mean-square (RMS) error of the output profile with respect of the target image, $RMS = \sqrt{\sum_{(y,z) \in MA} (I_o(y,z)/I_t(y,z) - 1)^2 / N}$ where N is the total number of pixels in the measurement area (MA), $I_o(y,z)$ and $I_t(y,z)$ are the output and target profiles with equalized energy. The simulation shows that the SLM-based pulse shaper illustrated in Fig. 1 converts the incident Gaussian pulse to the desired flattop pulse with a tapered end as shown in Fig. 2(a). The maximal intensity profile in the time x-z coordinates illustrates that the shaped pulse has a 45-degree tilt front [Figs. 2(c) and 2(d)]. The simulated shaped pulse in Figs. 2(e) and 2(f) shows a good conformity compared with the target profiles in Figs. 2(a) and 2(b) with a RMS error of 0.206 % over a 20.5×20.5 mm² square measurement area. Notice that, shown in Fig. 2, the beam profile is before the cylindrical lens.

Based on the above description for generating the tilt-front pulse with a tapered-end, the GENESIS code [18] is used for simulating the FEL process with the laser pulse acting as an effective optical undulator. GENESIS code for optical undulator is consistent with the analytical theory [5, 6] and the electromagnetic simulation code [4] established for an optical undulator.

As to the electron bunch parameter and quality, the laser-driven plasma accelerator can generate a high quality bunch [19]. The FEL gain process starts only on the flattop part of the laser as in Fig. 2(d), and no gain on the rising edge. With the parameters in Fig. 3, the FEL Pierce parameter is about $\rho \sim 0.0017$ [14], which characterizes the lasing efficiency $P_{\mathrm{FEL}} \approx \rho (\gamma m_e c^2 / e) I$ [14]. The GENESIS simulation gives a saturation power at the end of exponential growth of about $P_{\mathrm{sat}} \approx 120$ MW. The simulated FEL power for no taper case as the blue solid curve in Fig. 3 is consistent with the analytical estimate with 3-D gain length of $L_G = 0.44$ mm [14]. The FEL power for the tapered case (the red curve) is over 1 GW, about one order higher than that for the no tapered case. The wavelength spectrum shown in Fig. 3(b) represents a relative narrow bandwidth radiation. Fitting to a Gaussian envelop gives a FWHM relative bandwidth of 4.4×10^{-3} for a flattop electron bunch of about 100 fs duration. The far field transverse image is shown in Fig. 3(c) which is very close to a fundamental Gaussian mode with $M^2 \approx 1.03$ and transverse divergence $\sigma_{x'} \approx \sigma_{y'} \approx 86$ μrad and waist size of $w_0 = 4.9$ μm. In reality, the optical undulator is a Gaussian mode $E(x) = E_0 \exp[-x^2 / (4\sigma_{L,x}^2)]$ with E_0 the peak electric field and $\sigma_{L,x}$ the laser intensity rms x-size. The Gaussian distribution in the x-direction is similar to the transverse-gradient undulator [20], which can be used to compensate the energy spread of electron bunch if we inject the electron bunch with an x-offset from the laser center. We con-
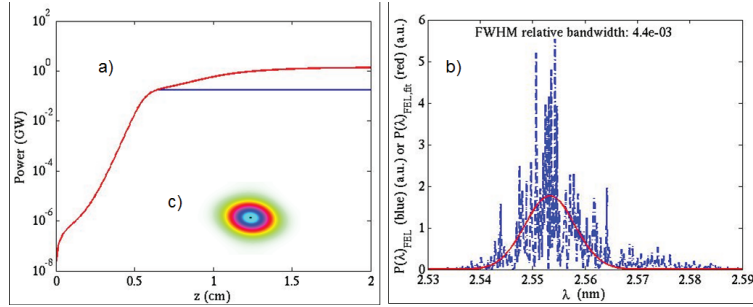

Fig. 3. (a) Radiation power without taper (blue curve) and with taper (red curve); (the length of taper L=2.3 cm, a = 0.4); (b) the spectrum; and c) Far field image of the X-ray pulse. The simulation parameters are: electron bunch central energy $\gamma = 80$, energy spread $\sigma_\gamma = 0.1$, normalized emittance $\varepsilon_N = 0.2$ π mm mrad, peak current $I = 3$ kA, beam transverse radius 5 μm, RMS $K = 1.5$, and the undulator period $\lambda_u = 10$ μm. There is no focusing magnet.

clude on the discussion of the peak brightness, defined as $B \equiv \dot{N}_{ph} / (4\pi^2 \sigma_T^2 \sigma_{T'}^2 d\omega / \omega)$ where T stands for x or y, i.e., the transverse dimension, $\sigma_{T'}$ for the RMS opening angle, $d\omega / \omega$ the relative bandwidth, and $\dot{N}_{ph}$ the flux of FEL. The peak brightness of the FEL pulse in our scheme achieves 10^{30} photons/mm^2/mrad^2/s/0.1% bandwidth, which is 10 orders (i.e., 10^{10} times) higher than the max theoretical brightness for the incoherent nonlinear Thompson Scattering [21] with only spontaneous radiation and no gain. Notice that, for undulator radiation the bandwidth of the central cone scales as $d\omega / \omega \sim 1/N_u$, and the RMS opening angle scales as $\sigma_{T'} = \sqrt{(1 + K^2) / (2N_u)} / \gamma$, thus, the brightness of X-ray is proportional to N_u^2. Therefore, even if there is no FEL-type exponential growth, the X-ray source's brightness benefits largely from the lengthened interaction time. For a sufficient long optical undulator with number of periods $N_u > 10 L_G / \lambda_u$, the interaction length can be 10-20 gain length, thus, with a high quality electron bunch, the high-gain Thompson Scattering FEL can be realized.

Acknowledgments